Author(s): Seo Yoon Junga, Yongmann M. Chung
Article Title: Large-eddy simulation of accelerated turbulent flow in a circular pipe
Year of publication: 2011
Link to published article:
http://dx.doi.org/10.1016/j.ijheatfluidflow.2011.11.005

Large-eddy simulation of accelerated turbulent flow in a circular pipe

Seo Yoon Jung[†] and Yongmann M. Chung[‡*]

† Department of Mechanical Engineering, Imperial College London, SW7 2AZ, U.K.

‡ School of Engineering and Centre for Scientific Computing, University of Warwick, Coventry, CV4 7AL, U.K.

[Revised Manuscript]

Abstract

Turbulent pipe flows subject to temporal acceleration have been considered in this study. Large-eddy simulations (LESs) of accelerated turbulent flow in a circular pipe were performed to study the response of the turbulent flow to temporal acceleration. The simulations were started with the fully-developed turbulent pipe flow at an initial Re number, and then a constant temporal acceleration was applied. During the acceleration, the Reynolds number of the pipe flow, based on the pipe diameter and the bulk-mean velocity, increased linearly from $Re_D = 7000$ to 36000. A dimensionless response time for various flow quantities was introduced to measure the delays in the response of the near-wall turbulence to temporal acceleration. The results reveal distinctive features of the delays responsible for turbulence production, energy redistribution, and radial propagation. The conditionally-averaged flow fields associated with Reynolds shear stress producing events were analysed. In the transient flows, sweeps and ejections were closely linked to the delays of turbulence production and of turbulence propagation away from

*Corresponding author: Y.M.Chung@warwick.ac.uk

the wall. It is found that strong sweep events were related to the delayed turbulence production in the near-wall region, while ejection events were associated with the propagation of the turbulence away from the wall. The results show that the anisotropy of the turbulence was enhanced during the transient, and this would be a challenging problem to standard turbulence models.

Keywords: pipe flow; transient; large-eddy simulation; acceleration; turbulence; delay effect

1 Introduction

Unsteady turbulent flows through a pipe are frequently encountered in engineering applications such as turbo-machinery and heat exchangers, and also in biomedical applications such as airflow in the human lungs and blood flow in large arteries. In addition to the practical implications of achieving a better understanding of flows of this type, the study of unsteady turbulent flows in pipes provides insight into the underlying physics of turbulent boundary layers. To date, unsteady turbulent pipe flows have received relatively little attention compared to steady ones despite their importance.

Many experimental and numerical studies of unsteady turbulent pipe (Mizushina et al., 1973; Ramaprian and Tu, 1983; Shemer et al., 1985) and channel (Tardu et al., 1994; Scotti and Piomelli, 2001, 2002) flows have focused on periodic pulsating flows rather than non-periodic transient ones due to their practical applications concerned and the easy generation of the periodic flows. Mizushina et al. (1973), Ramaprian and Tu (1983), Shemer et al. (1985), and Tardu et al. (1994) have found that, in pulsating turbulent flow experiments, the effects of the pulsation frequency and the mean flow rate were significant to the turbulence whereas that of amplitude was small. Scotti and Piomelli (2001, 2002) performed a large-eddy simulations (LES) of pulsating channel flow and subsequently tested the capability of Reynolds-avegared Navier-Stokes (RANS) equations simulations. They found that the near-wall turbulence generated by the unsteady pressure gradient did not propagate beyond a certain distance l_t and that the $k - \varepsilon - v^2$ turbulence model performed better than other RANS models tested.

As regards the non-periodic transient pipe flow, Kataoka et al. (1975) have investigated the response to a step input of flow rate using an electrochemical technique. They found that the time at which transition from laminar to turbulent state occurred decreased with increasing Reynolds number. Maruyama et al. (1976) carried out an experiment in similar conditions to that of Kataoka et al. (1975). They observed the delay in the response of turbulence, which was found to propagate from the wall to the centre of the pipe. A study of He and Jackson (2000) was concerned with flow transients with increasing and decreasing flow rates in a pipe using laser doppler velocimetry. They ob-

served three delays in the turbulence: a delay in the turbulence production, a delay in turbulence energy redistribution, and a delay related to the radial propagation of turbulence. Moreover, they found that the radial propagation of turbulence was determined by initial flow conditions. Greenblatt and Moss (2004) measured the turbulent pipe flow with a temporal pressure gradient change which was larger than those considered in the previous studies (Maruyama et al., 1976; He and Jackson, 2000). They divided the flow regime into four different phases and identified the reconstitution of the wake, which was not observed in the previous studies.

Numerical studies on the transient turbulent flow with temporal pressure gradient are relatively scarce. A direct numerical simulation (DNS) of a decelerated turbulent channel flow subjected to a sudden change of pressure gradient was performed by Chung (2005, 2006). He found that there are two different relaxations in the decelerated flow: a fast relaxation at the early stage and a slow one at the later stage. The anisotropic response of the near-wall turbulence was detected in the early stage, which would be a troublesome problem to standard turbulence models (Chung and Jafarian, 2005; He et al., 2008; Khaleghi et al., 2009). Chung and Jafarian (2005) applied several turbulence models to the decelerated flow with mixed success.

In the present work, large-eddy simulations of an accelerated turbulent pipe flow were performed to elucidate the delay effect on the near-wall turbulence. This is, to the best knowledge of the authors, the first LES study of the turbulent pipe flow with temporal acceleration. The simulation conditions were chosen to be the same as in the experiments of He and Jackson (2000). Various turbulence statistics were analysed to study the response of the near-wall turbulent flow. A dimensionless time for the response of turbulence is proposed to shed light on the delay effect. The results can be useful for the development of better turbulence models for transient flows.

2 Numerical methods

The governing equations for LES are the filtered continuity and incompressible Navier-Stokes equations:

$$\frac{\partial \overline{u}_i}{\partial x_i} = 0, \tag{1}$$

$$\frac{\partial \overline{u}_i}{\partial t} + \frac{\partial}{\partial x_j}\left(\overline{u}_i \overline{u}_j\right) = -\frac{\partial \overline{p}}{\partial x_i} + \frac{1}{Re}\frac{\partial^2 \overline{u}_i}{\partial x_j \partial x_j} - \frac{\partial \tau_{ij}}{\partial x_i}, \tag{2}$$

where an overbar denotes filtered variables, and τ_{ij} is the subgrid-scale stress:

$$\tau_{ij} = \overline{u_i u_j} - \overline{u}_i \overline{u}_j. \tag{3}$$

All variables are non-dimensionalised by the pipe radius, R, and the bulk-mean velocity at the initial Reynolds number, U_{m0}. The subscript 0 indicates values at the initial Reynolds number. As for the coordinates, x, r and θ are the axial, radial and circumferential directions, respectively, and u, u_r and w are the corresponding velocity components. For comparison with other wall-bounded turbulent flows, an additional coordinate is introduced: $y = R - r$, and $v = -u_r$, where y is the wall-normal coordinate, and v the corresponding velocity component. The origin of the coordinate is located at the centre of inlet plane at $x = 0$.

In the present study, the simulations were started from a fully-developed turbulent pipe flow at $Re_{D0} = 7000$, where the Reynolds number ($Re_D = U_m D/\nu$) is based on the pipe diameter and the bulk-mean velocity. The acceleration parameter, $f = dU_m/dt$, is introduced to represent the non-dimensional change in the bulk-mean velocity. The mean pressure gradient was dynamically adjusted during the acceleration, so that the bulk-mean velocity increased linearly in time at a prescribed rate. When $f = 0$, this procedure was the same as the method used in a constant mass flow rate simulation. The acceleration parameter, f, was kept constant throughout the simulations, so the mass flow rate was increased linearly to the final Reynolds number of $Re_{D1} = 36000$. The acceleration parameter was chosen as $f = 0.2$ to compare the results with the experimental data of He and Jackson (2000). In the experiment, the water flow in a pipe of

diameter 50.8mm was accelerated from $Re_{D0} = 7000$ to $Re_{D1} = 45200$ over 5 seconds; the corresponding dimensionless ramp rate parameter is $\gamma = D/u_{\tau_0}(1/U_{m0} \cdot dU_m/dt) = 6.1$, and they used this parameter as an indication of the departure from the turbulence of pseudo-steady flow. Much weaker ramp rate parameters were also used in the experiment, but comparison was restricted to the $f = 0.2$ case due to computational constraints.

Numerical methods in cylindrical coordinates require significant effort to treat the singularity at $r = 0$. In the present formulation, the radial flux $q_r = ru_r$ on a staggered grid was introduced to simplify the discretisation of this region, since $q_r = 0$ at $r = 0$ (Verzicco and Orlandi, 1996). Periodic boundary conditions were applied in the axial and circumferential directions, and a no-slip boundary condition was imposed at the walls.

A dynamic subgrid-scale model (Germano et al., 1991; Lilly, 1992) was used to account for subgrid-scale stresses. Using the eddy-viscosity assumption, the turbulent eddy viscosity ν_t was expressed as $\nu_t = C_s\overline{\Delta}^2|\overline{S}|$, where $|\overline{S}| = \sqrt{2\overline{S}_{ij}\overline{S}_{ij}}$. In this study, the model coefficient C_s was determined using the dynamic eddy viscosity model proposed by Germano et al. (1991), as modified and extended by Lilly (1992). In this model, the constant C_s is not given a priori, but is computed from the flow variables during the simulation. The model constant C_s was averaged over the x and θ directions. A detailed description of the method for determining the model coefficient can be found in the papers of Germano et al. (1991) and Lilly (1992). The grid filter width Δ was taken to be equal to the grid spacing. The box filter was applied in the streamwise and azimuthal directions for the test filter (Lund, 1997). No explicit test filtering was applied in the radial direction. The total viscosity, $\nu + \nu_t$, was constrained to be non-negative to ensure numerical stability of the time integration (Germano et al., 1991).

The governing equations were integrated in time using the fractional step method with the implicit velocity decoupling procedure proposed by Kim et al. (2002). In this approach, the terms in the momentum equations were first discretised in time using the Crank-Nicolson method, and then the coupled velocity components in the convection terms were decoupled using the implicit velocity decoupling procedure. The decoupled velocity components were then solved without iteration. Because the implicit decoupling procedure relieved the Courant-Friedrichs-Lewy (CFL) restriction, the computation time

was reduced significantly. In the preliminary calculation of the present flow configuration, the comparison between the iterative numerical scheme (Choi and Moin, 1994) and the present one was made. Usually, three or four iterations were needed to obtain a converged solution with the coupled velocity components, and the computational time of the iterative scheme was $1.6 \sim 1.9$ times larger than that of Kim et al. (2002). The overall accuracy of the present numerical methods was second-order in time. All terms were resolved using a second-order central difference scheme in space on a staggered mesh. Details regarding the numerical algorithm can be found in Kim et al. (2002).

3 Results and Discussion

First, a DNS of steady turbulent pipe flow at $Re_D = 5300$ was conducted to ascertain the reliability and accuracy of the present numerical methods. The computational domain length was $10R$ in the streamwise direction and the grid points used were $257(x) \times 69(r) \times 129(\theta)$. The domain size and the grid resolution were the same as in the DNS of Akselvoll and Moin (1996). As shown in Figure 1, the root-mean-squared (rms) velocity fluctuations ($u_{i,rms}$) are in excellent agreement with the previous DNS data of Akselvoll and Moin (1996), demonstrating that the numerical methods employed in this study are adequate for the steady turbulent pipe flow simulation.

In the accelerated turbulent flow, the Re number increases in time, and consequently, the grid resolution calculated in local wall units varied during the simulation. The grid resolution was finest at the initial Re number, and even comparable to the one used in the DNS of Akselvoll and Moin (1996). Then, the grid resolution became coarser with the increase of Re, and would eventually become too coarse to resolve turbulent structures. To find the Re number range which could be resolved accurately, preliminary simulations of transient turbulent pipe flow were performed with 6.3×10^6 (medium) and 8.4×10^6 (fine) grid points (Jung and Chung, 2007, 2009; Chung, 2008). The domain sizes of $L = 10R$ was used for the medium grid while $L = 8R$ was used for the fine grid to improve the resolution. For this test, the same initial Re number of $Re_{D0} = 7000$ and the acceleration parameter of $f = 0.2$ were used. The simulations were run up to a non-dimensional time

$T_e = 27.2R/U_{m0}$ with a final Re number of $Re_D = 45200$. From the preliminary tests, little difference was observed between the simulations for $7000 \leq Re_D \leq 36000$, and a small difference appeared only at the later stage of transient, where the Re numbers were relatively high ($Re_D > 36000$).

The results presented in this paper were obtained with the 8.4×10^6 grid points for $7000 \leq Re_D \leq 36000$. The computational domain in the streamwise direction was $L = 8R$. The number of grid points used was $128 \times 256 \times 256$ in the x, r, and θ directions, respectively. In the wall-normal direction, grid points were clustered according to a hyperbolic tangent distribution. The grid resolution at the initial Re number ($Re_{D0} = 7000$) was $\Delta x^+ = 14.38$, $\Delta y^+_{min} = 0.02$, $\Delta y^+_{max} = 2.9$, and $\Delta z^+_{max} (\equiv R\Delta\theta^+) = 5.65$. This is comparable to the resolution used in the DNS of Akselvoll and Moin (1996), indicating that the grid resolution is very fine at the initial Re number. At the final Reynolds numbers ($Re_{D1} = 36000$), the resolution was $\Delta x^+ = 61.0$, $\Delta y^+_{min} = 0.08$, $\Delta y^+_{max} = 12.2$, and $\Delta z^+_{max} = 23.95$. A time step size of $0.0005R/U_{m0}$ was used and the total excursion time was $T_e = 20.6R/U_{m0}$. All statistics were obtained using plane averaging in the streamwise and azimuthal directions. The ensemble averages were based on databases consisting of eight independent realisations.

3.1 Transient

An LES of steady pipe flow at $Re_D = 7000$ was performed to provide the initial conditions for the main simulations. The corresponding Re number based on the friction velocity was $Re_\tau = 230$. The mean velocity (U_m) and rms fluctuations ($u_{i,rms}$) compared very well with the DNS results of $Re_D = 5300$ as shwon in Figure 1. Now, the flow rate of the pipe flow was increased linearly in time from the initial value of $Re_D = 7000$ to the final value of $Re_D = 36000$ (or $Re_\tau = 960$) over a total excursion time of $T_e = 20.6R/U_{m0}$.

Figure 2 shows the temporal development of the skin friction coefficient, $C_f = \tau_w/(\frac{1}{2}U_m^2)$, during the transient period. Blasius' law of $C_f = 0.0791 Re_D^{-1/4}$ is employed to compare the present results with those of the steady pipe flow. LES results of steady pipe flow at five Re_D numbers are also included in the figure for comparison. As shown in Figure 2,

the response of the wall shear stress to the temporal acceleration is rather complex, and can be divided into three different stages: an initial weak time-dependence (WT) stage, a strong time-dependence (ST) stage, and a pseudo-steady (PS) stage. Note that the local Reynolds number is equivalent to the time elapsed after the onset of the acceleration since the mass flow rate increases linearly in time: $Re_D = Re_{D0} + (Re_{D1} - Re_{D0})\xi/T_e$, where ξ is the time measured from the onset of the acceleration.

In the initial WT stage ($7000 < Re_D < 21000$, or $0 < \xi < 10$), the main feature is a delay effect. The increase in the wall shear stress is much weaker than the steady pipe flow case, and the rate of change in the wall shear stress ($d\tau_w/dt$) is roughly half of the corresponding steady value. At the end of the WT stage ($Re_D = 21000$), C_f is about 70% of the corresponding steady value due to the slow response of the near-wall turbulence (He and Jackson, 2000). During the ST stage ($21000 < Re_D < 28000$, or $10 < \xi < 15$), the most striking feature is a rapid increase in C_f. The rate of change in the wall shear stress is twice as high as the steady value, and this suggests that turbulence production near the wall is significantly enhanced at this stage. At the end of the ST stage ($\xi = 15$), the C_f value has recovered almost the corresponding steady value at $Re_D = 28000$. In the PS stage ($Re_D > 28000$, or $\xi > 15$), the skin-friction decreases at the same rate as in the steady state case, and this indicates that the near-wall turbulence has approached the pseudo-steady state. Note that the classification in Figure 2 is based on the skin friction, and it represents the response of near-wall turbulence. As shown later, however, the response of turbulence away from the near-wall region is much slower, and the pseudo-steady state is not achieved until much later at $\xi = 20$ (or $Re_D = 35000$).

3.2 Mean velocity

Figure 3 shows the local mean streamwise velocity profiles at several time instants during the acceleration with the experimental data of He and Jackson (2000). It is worth noting that near-wall measurement ($y/R < 0.55$) is not available in their experiment. The numerical results are in good agreement with the experimental data. During the acceleration, the local bulk-mean velocity has increased by about 5.1 times. In the WT

stage, it is clear that the local bulk-mean velocity increases by the same amount in all radial locations apart from the near-wall region ($y < 0.1$). As the influence of the wall grows in the ST stage, the rate of increase starts to reduce in most areas apart from the pipe centre region. In the experiment of He and Jackson (2000), the streamwise velocity was measured at 12 radial locations, and the first measurement location was at $y = 0.055$, which corresponds to $y^+ = 13$ at $Re_{D0} = 7000$, and $y^+ = 53$ at $Re_{D1} = 36000$. This location lies outside the buffer layer, where most near-wall turbulence production takes place. So, the temporal development of the near-wall turbulence (in the viscous sublayer and the buffer layer) can not be compared directly with the measurements of He and Jackson (2000).

Figure 4 shows the mean velocity at several time instants, using wall units $u^+ = u/u_\tau$ and $y^+ = yu_\tau/\nu$, where u_τ is the local friction velocity. There is an undershoot in the log-law profile in the early WT stage ($Re_D = 7350$) due to the sudden increase in u_τ as shown in Figure 2. As the wall shear stress has not recovered its steady value, an overshoot in the velocity profiles is observed in the late WT stage and the ST stage ($Re_D = 14000$ and 21000). As expected, the mean velocity follows the steady profile in the PS stage. It is worthwhile to mention that some similarities between temporally accelerating flow and spatially accelerating flow have been observed in this study. For example, the local log-law profiles showed an overshoot in the early transient region of the favourable pressure-gradient boundary layer (Fernholz and Warnack, 1998; Piomelli et al., 2000).

3.3 Velocity fluctuations

The rms velocity fluctuations are shown in Figure 5. The velocities are normalised by the initial bulk-mean velocity, $u_{i,rms}/U_{m0}$. One of the important features of the response of velocity fluctuations to the acceleration is a delay effect (He and Jackson, 2000; Jung and Chung, 2009). It is clear from Figure 5 that the magnitudes of all velocity fluctuations change very little during the early WT period, indicating that the turbulence is frozen in this early stage. When the turbulence intensities are normalised by the local bulk-mean

velocity, $u_{i,rms}/U_m$ is actually attenuated, as pointed out in the previous studies (He and Jackson, 2000; Jung and Chung, 2009). This clearly indicate that turbulence production is delayed at the WT stage of the transient (see also Figure 6).

It is found that the response to the temporal acceleration of different velocity components is different from each other, although the v_{rms} and w_{rms} components display similar behaviour. In the wall region ($y < 0.2$), u_{rms} increases after the initial delay whereas v_{rms} and w_{rms} do not change much in the WT stage. This suggests that the anisotropy of the turbulence near the wall becomes manifest during the transient moving towards to a single component state, which would be a challenge to conventional turbulence models (Chung and Jafarian, 2005; Khaleghi et al., 2009). The axial velocity fluctuations first respond to the temporal acceleration: A strong increase in u_{rms} occurs in the near-wall region, and this is closely associated with the turbulence production near the wall. The radial and azimuthal velocity fluctuations shown in Figures 5b and 5c also show delayed responses. Compared to the axial velocity fluctuations, v_{rms} and w_{rms} exhibit longer delays, and this can be explained by the fact that these velocity components have no production term in their transport equations (Mansour et al., 1988; Chung, 2005). As a result, v_{rms} and w_{rms} start to increase much later, and the energy redistribution mechanism between velocity components is responsible for the delayed increase in v_{rms} and w_{rms} (He and Jackson, 2000).

To achieve a better understanding of transient turbulent flows, the relative rate of change of rms velocity fluctuations is calculated from Figure 5. The non-dimensional rate of change of a flow quantity ϕ is defined as:

$$g(\phi) = \frac{R}{U_{m0}\phi_t}\frac{\phi_{t+\Delta t} - \phi_t}{\Delta t}, \tag{4}$$

where $\Delta t = 0.25R/U_{m0}$ is chosen to evaluate the time derivative. It is found that all three velocity components increase drastically very close to the wall ($y < 0.05$) for $20000 < Re_D < 25000$. This reflects the augmentation of turbulence production and energy redistribution in this region. The increased near-wall turbulence generation propagates towards the pipe centre in both the ST and PS stages, displaying a banded region

of high rate of change from the wall to the pipe centre, which represents the radial propagation of turbulence. This radial propagation explains the delay in the core region ($y > 0.2$) (Maruyama et al., 1976; He and Jackson, 2000).

Figure 6 shows the production term in the turbulence kinetic energy transport equation in local wall units, $-\overline{u'v'}(dU/dy)\nu/u_\tau^4$. The delay effect and the non-equilibrium state of turbulence are again evident in the production term. In the early WT stage, the production term is frozen due to the slow response of the Reynolds shear stress and the mean velocity field, and the location of the peak does not change in time but remains at the initial location. When expressed in local wall units, however, the peak location moves gradually away from the wall, and the magnitude of the production decreases due to the increase in u_τ. The production term starts to increase at $Re_D = 10000$, and this is when the u_{rms} component begins to increase. As the near-wall turbulence activities become stronger in the ST stage, the location of the peak moves towards the wall, and the peak is located at around $y^+ = 12$ in the PS stage as in the steady turbulent boundary layer (Kim et al., 1987), indicating that the near-wall turbulence has recovered the equilibrium state.

Figure 7 displays the rms velocity fluctuations near the wall along with the experimental data of He and Jackson (2000). It is worth noting that there is a significant difference in the initial rms velocity fluctuations between the LES and the experiment: The initial rms values of the experiment, v_{rms} and w_{rms} in particular, are found to be much larger than the available DNS data at a similar Re number, while the initial condition used in this study compares very well with the DNS data as shown in Figure 1. The noise in the LDA signal in the experiment could have contributed to high levels of Reynolds normal stresses. Considering this difference, there is reasonably good qualitative agreement between the LES results with the experimental data. The delay effect in the WT stage is clearly seen in all three velocity components. In Figure 7a, the magnitude of the axial velocity fluctuations changes gradually during the WT stage, followed by a rapid increase in the ST stage. As mentioned above when discussing Figure 6, this rapid increase of the axial velocity fluctuations is closely associated with the near-wall turbulence production (He and Jackson, 2000; Jung and Chung, 2009). It is also interesting to note that the

delay in the early WT stage is rather short at $y = 0.075$, while there is a longer delay at $y = 0.173$. It should be noted that $y = 0.075$ and $y = 0.173$ corresponds to $y_0^+ = 17$ and 40, based on the initial friction velocity. It is found that the delay time for the u_{rms} component in the wall region ($y < 0.2$) increases with the distance from the wall (see also Figure 9).

It is worth mentioning that a plateau in the near-wall axial velocity fluctuations at $y = 0.075$ is correctly predicted in the ST stage (Figure 7a). This plateau region can be explained by the development of u_{rms} profiles for $24500 < Re_D < 28000$. It is found that the u_{rms} fluctuations at $y = 0.075$ remain unchanged in this Re range while near the wall ($y < 0.075$), u_{rms} increases with increasing Re due to the enhancement of new turbulence production. The maximum u_{rms} value increases by 10% during this period and its location moves towards the wall while the local friction velocity, u_τ, increases by 20%.

The radial and azimuthal velocity fluctuations shown in Figures 7b and 7c exhibit delayed responses, and the delay in the v_{rms} and w_{rms} components are much longer than that of u_{rms}, apart from the pipe centre region, where similar delays are observed in all three velocity components. After the onset of the acceleration, v_{rms} and w_{rms} remain constant for most part of the WT stage, and this delay is attributed to the lack of the production terms in their transport equations (He and Jackson, 2000). It is worth noting that, unlike u_{rms}, the behaviour of v_{rms} and w_{rms} at the two radial locations ($y = 0.075$ and 0.173) shows similar trends to each other, demonstrating different responses of the velocity fluctuations to the acceleration.

The behaviour of the Reynolds shear stress, $-\overline{u'v'}$, is found to be similar to that of v_{rms} and w_{rms}. Figure 8 shows the Reynolds shear stress normalised by the initial bulk-mean velocity, $-\overline{u'v'}/U_{m0}^2$. $-\overline{u'v'}$ exhibits a significant delay and does not change in the early WT stage. This clearly shows that the turbulence is slower to respond to the acceleration than the mean velocity, and becomes less efficient to extract energy from the mean flow field in the WT stage. This becomes clearer when the local bulk-mean velocity is used instead of the initial bulk-mean velocity: $-\overline{u'v'}/U_m^2$ decreases in the WT stage due to the linear increase in the local bulk-mean velocity (Jung and Chung, 2009).

After the initial delay, $-\overline{u'v'}$ starts to increase at $Re_D = 17000$. It is interesting to note that this Reynolds number is roughly when v_{rms} and w_{rms} also begin to increase.

3.4 Time delay

To obtain a quantitative measure of the time delay in the response of a flow variable, dimensionless delay time ξ^* corresponding to $(\phi - \phi_0)/\phi_0 > a_\phi$ is calculated as a function of its distance from the wall in Figure 9. Greenblatt and Moss Greenblatt and Moss (2004) used a threshold value of $a_\phi = 0.15$ in their analysis. To find an appropriate threshold value for a_ϕ, values in the range of $0.15 \leq a_\phi \leq 0.8$ were tested in this study. Although similar results were obtained for $a_\phi = 0.15$, 0.5 and 0.8, with a small value of a_ϕ being associated with a short delay, $a_\phi = 0.8$ was found to show the most similar trend of delay and propagation characteristics shown in Figures 5 and 7. The mean velocity shows the fastest response among all flow quantities in Figure 9. In the pipe centre region, the delay time of U_m is about $\xi^* = 5.5R/U_{m0}$, while the near-wall region has a delay time of $\xi^* = 2.7R/U_{m0}$. It is worth noting that the delay time for the bulk-mean velocity is about $\xi^* = 3.4R/U_{m0}$, which is a little larger than the near-wall delay time, and much smaller than the centre-line velocity delay time. It is notable that apart from the wall region there is relatively small variation of the response of the mean velocity along the radial direction when compared to the variations of velocity fluctuations. This is consistent with the findings in Figure 3 that the mean velocity responds to the acceleration like a slug flow (He and Jackson, 2000).

Unlike the mean velocity, the changes in the velocity fluctuations are gradual and much slower. Turbulence is observed to increases in the near-wall region first, and then propagates towards the pipe centre. This is clearly seen in Figure 9, where the delay time increases almost linearly with the distance from the nearest wall for $0.2 < y < 0.7$. However, this linear behaviour does not continue in the pipe centre region ($y > 0.7$). Instead, the delay time in the pipe centre region ($y > 0.7$) is found to be much smaller than expected from the linear relationship. This is because the flow in the pipe centre region is influenced by the propagation from all radial directions. It should also be

noted that away from the wall, the propagation speeds of the three velocity components are almost the same in the ST stage. For $0.2 < y < 0.7$, the response of the velocity fluctuations propagates from the wall to the pipe centre at the speed of $c = 0.1U_{m0}$ or $c_0^+ = 1.5$ (based on u_{τ_0}). The propagation starts at $Re_D = 21000$ or $\xi = 10$, so the propagation velocity based on $Re_D = 21000$ is about $c^+ = 0.7$. It is interesting to note that the new turbulence structures propagated at a constant speed in the acceleration phase of the pulsating turbulent channel flow (Scotti and Piomelli, 2001). At low pulsating frequencies, the propagation speed in the pulsating flow was $c^+ = 2\kappa$, where κ is the von Karman constant. However, a direct comparison should be taken with caution due to the obvious differences between the two cases.

In the wall region ($y < 0.2$), u_{rms} responds to the imposed acceleration first and then v_{rms} and w_{rms} follow. This tendency represents the delays of turbulence production for u_{rms}, and of energy redistribution by pressure strain for v_{rms} and w_{rms}. The axial component of turbulent energy is directly supplied from the mean flow through the mean shear and the Reynolds shear stress, while the main source of the radial and azimuthal components of turbulent energy stems from the redistribution of the axial component by the pressure strain mechanism. It is found that the delay time for the u_{rms} component in the wall region ($y < 0.2$) increases almost linearly away from the wall (see Figure 9). The propagation speed of u_{rms} in the wall region ($y < 0.2$) is about $c_x = 0.03U_{m0}$ or $0.5u_{\tau_0}$, a third of the core region value. This explains the differences in the response of u_{rms} at two locations ($y = 0.075$ and 0.173), as shown in Figure 7a. The delay between the two locations ($d = 0.098$) is $\Delta\tau = d/c_x = 3.3$, and this delay time is equivalent to $\Delta Re_D = 4500$ in Reynolds number difference, as shown in Figure 7a. The near-wall responses of the v_{rms} and w_{rms} components are even slower than u_{rms} very near the wall due to the lack of turbulence production. This is consistent with the findings in Figures 5 and 7. At $y < 0.05$, the propagation speed of v_{rms} is about $c_y = 0.01U_{m0}$ or $0.15u_{\tau_0}$, but for $0.05 < y < 0.2$ the propagation speeds of v_{rms} and w_{rms} are much faster than the u_{rms} value.

3.5 Quadrant analysis

Quadrant analysis of the Reynolds shear stress $-\overline{u'v'}$ provides detailed information on the contribution of flow events to the production (or destruction) of turbulent kinetic energy (Willmarth and Lu, 1972; Brodkey et al., 1974). The analysis divides the Reynolds shear stress into four categories according to the signs of u_{rms} and v_{rms}. The first quadrant (Q1), $u' > 0$ and $v' > 0$, contains outward motion of high-speed fluid; the second quadrant (Q2), $u' < 0$ and $v' > 0$, contains outward motion of low-speed fluid referred to as the ejection events; the third quadrant (Q3), $u' < 0$ and $v' < 0$, contains inward motion of low-speed fluid; the fourth quadrant (Q4), $u' > 0$ and $v' < 0$, contains an inrush of high-speed fluid referred to as the sweep events. Here, Q1 and Q3 events contribute to the negative Reynolds shear stress (negative production) while Q2 and Q4 events contribute to the positive Reynolds shear stress (positive production).

The contribution to the Reynolds shear stress from each quadrant is shown in Figure 10. Here, the local friction velocity has been used to calculate y^+ values. The crossover point between the dominance of Q2 and Q4 events is located at $y^+ \approx 13$ for $Re_D = 7000$. This is very similar to the numerical results for turbulent channel flow (Kim et al., 1987), indicating that the initial near-wall turbulence is in the equilibrium state. It is notable that the position of the crossover point moves away from the wall with increasing Reynolds number. The Q4 events near the wall increase gradually with the introduction of the acceleration, and strong Q4 events take place in the late WT and early ST stages ($17500 \leq Re_D \leq 24500$). The contribution of Q4 becomes much larger than that of Q2 at the end of the WT stage at $Re_D = 21000$.

The joint weighted probability density functions (pdf) are also examined at $y = 0.04$ and 0.5 in Figure 11. The $y = 0.04$ location corresponds to $y^+ = 9$ at $Re_{D0} = 7000$, and $y^+ = 20$ at $Re_{D1} = 21000$. The pdf results in Figure 11a show that the increase in Q4 is attributed mainly to the large amplitude of the radial velocity fluctuations, and this indicates that the strong Q4 events in the transient flow are closely related to the sudden change in near-wall turbulence (Figures 5 and 7). However, the large increase in near-wall v_{rms} could not be detected in the previous experiment of He and Jackson (2000)

due to measurement constraints. From the pdf study in Figure 11b, it is also found that strong Q2 events occur in the ST stage ($21000 \leq Re_D \leq 28000$) away from the wall. This suggests that Q2 events are associated with the propagation of turbulence from the wall towards the pipe centre.

4 Conclusions

In this study, numerical simulations of transient turbulent pipe flow were performed using LES to investigate the response of unsteady turbulence to temporal acceleration. The response of the transient flow after the onset of the acceleration was divided into three stages, based on the unsteady skin-friction behaviour: weak time-dependence (WT), strong time-dependence (ST), and pseudo-steady (PS) stages. After an initial delay, flow quantities increased rapidly in the ST stage, and recovered almost the corresponding steady value at the end of the ST stage. From the analysis of velocity fluctuations, three delays responsible for the turbulence production, energy redistribution, and radial propagation were identified. A dimensionless time for the response of turbulence was employed to quantify the delay effects, and the speed of the radial propagation was found to be $c_0^+ = 1.5u_{\tau_0}$ in the core region ($0.2 < y < 0.7$). The conditionally-averaged flow fields associated with Reynolds shear stress producing events showed that sweeps and ejections were closely related to the delays of turbulence production and the turbulence propagation towards the pipe centre. It was found that the anisotropy of the turbulence was enhanced during the acceleration. Some similarities between temporally accelerating flow and spatially accelerating flow have been observed in this study.

Acknowledgements

This work was supported by the Engineering and Physical Sciences Research Council (EPSRC) through the UK Turbulence Consortium (Grant EP/G069581/1). Computer resources were provided by the Centre for Scientific Computing, University of Warwick. SYJ was supported by the Korea Research Foundation (KRF-2006-214-D00018).

References

K. Akselvoll and P. Moin. An efficient method for temporal integration of the Navier-Stokes equations in confined axisymmetric geometries. *Journal of Computational Physics*, 125(2):454–463, 1996.

R. S. Brodkey, J. M. Wallace, and H. Eckelmann. Some properties of truncated turbulence signals in bounded shear flows. *Journal of Fluid Mechanics*, 63(part 2):209–224, 1974.

H. Choi and P. Moin. Effects of the computational time step on numerical solutions of turbulent flow. *Journal of Computational Physics*, 113(1):1–4, 1994.

Y. M. Chung. Unsteady turbulent flow with sudden pressure gradient changes. *International Jounal for Numerical Methods in Fluids*, 47(8-9):925–930, 2005.

Y. M. Chung. Numerical simulations of transient turbulent flows. In *6th European Fluid Mechanics Conference*, Stockholm, Sweden, 2006.

Y. M. Chung. Response of near-wall turbulent flow to temporal acceleration. In *7th European Fluid Mechanics Conference*, volume 1, page 165, Manchester, U.K., 2008.

Y. M. Chung and M. M. Jafarian. Direct numerical simulation of unsteady decelerateing. In J. A. C. Humphrey, T. B. gatski, J. K. Eaton, R. Friedrich, N. Kasagi, and M. A. Leschziner, editors, *Turbulence and Shear Flow Phenomena -4*, volume 1, pages 319–324, 2005.

H. H. Fernholz and D. Warnack. The effects of a favourable pressure gradient and of the Reynolds number on an incompressible axisymmetric turbulent boundary layer. Part 1: The turbulent boundary layer. *Journal of Fluid Mechanics*, 359:329–356, 1998.

M. Germano, U. Piomelli, P. Moin, and W. H. Cabot. A dynamic subgrid-scale eddy viscosity model. *Physics of Fluids A*, 3(7):1760–1765, 1991.

D. Greenblatt and E. A. Moss. Rapid temporal acceleration of a turbulent pipe flow. *Journal of Fluid Mechanics*, 514:65–75, 2004.

S. He and J. D. Jackson. A study of turbulence under conditions of transient flow in a pipe. *Journal of Fluid Mechanics*, 408:1–38, 2000.

S. He, C. Ariyaratne, and A. E. Vardy. A computational study of wall friction and turbulence dynamics in accelerating pipe flows. *Computers and Fluids*, 37(6):674–689, 2008.

S. Y. Jung and Y. M. Chung. LES of transient turbulent flow in a pipe. In *11th European Turbulence Conference*, page 781, 2007.

S. Y. Jung and Y. M. Chung. Large-eddy simulation of accelerated turbulent flow in a pipe. In *Turbulence and Shear Flow Phenomena -6*, volume 1, pages 277–282, 2009.

K. Kataoka, T. Kawabata, and K. Miki. The start-up response of pipe flow to a step change in flow rate. *Journal of Chemical Engineering Japan*, 8(4):266–271, 1975.

A. Khaleghi, M. Pasandideh-Frad, M. M. Jafarian, and Y. M. Chung. Assessment of common turbulence models under conditions of temporal acceleration in a pipe. *Journal of Applied Fluid Mechanics*, 4(1):25–33, 2009.

J. Kim, P. Moin, and R. Moser. Turbulence statistics in fully developed channel flow at low Reynolds number. *Journal of Fluid Mechanics*, 177:133–166, 1987.

K. Kim, S.-J. Baek, and H. J. Sung. An implicit velocity decoupling procedure for the incompressible Navier-Stokes equations. *International Jounal for Numerical Methods in Fluids*, 38(2):125–138, 2002.

D. K. Lilly. A proposed modification of the Germano subgrid-scale closure method. *Physics of Fluids A*, 4(3):633–635, 1992.

T. S. Lund. On the use of discrete filters for large eddy simulation. Annual Research Briefs, Center for Turbulence Research, NASA Ames/Stanford University, pages 83–95, 1997.

N. N. Mansour, J. Kim, and P. Moin. Reynolds-stress and dissipation-rate budgets in a turbulent channel flow. *Journal of Fluid Mechanics*, 194:15–44, 1988.

T. Maruyama, T. Kuribayashi, and T. Mizushina. The structure of the turbulence in transient flows. *Journal of Chemical Engineering Japan*, 9:431–439, 1976.

T. Mizushina, T. Maruyama, and Y. Shiozaki. Pulsating turbulent flow in a tube. *Journal of Chemical Engineering Japan*, 6:487–494, 1973.

U. Piomelli, E. Balaras, and A. Pascarelli. Turbulent structures in accelerating boundary layers. *Journal of Turbulence*, 1(1):1–16, 2000.

B. R. Ramaprian and S. W. Tu. Fully developed periodic turbulent pipe flow. Part 2: The detailed structure of the flow. *Journal of Fluid Mechanics*, 137:59–81, 1983.

A. Scotti and U. Piomelli. Numerical simulation of pulsating turbulent channel flow. *Physics of Fluids*, 13(5):1367–1384, 2001.

A. Scotti and U. Piomelli. Turbulence models in pulsating flows. *AIAA Journal*, 40(3): 537–543, 2002.

L. Shemer, I. Wygnanski, and E. Kit. Pulsating flow in a tube. *Journal of Fluid Mechanics*, 153:313–337, 1985.

S. F. Tardu, G. Binder, and R. F. Blackwelder. Turbulent channel flow with large amplitude. *Journal of Fluid Mechanics*, 267:109–151, 1994.

R. Verzicco and P. Orlandi. A finite-difference scheme for three-dimensional incompressible flows in cylindrical coordinates. *Journal of Computational Physics*, 123(2):402–414, 1996.

W. W. Willmarth and S. S. Lu. Structure of the Reynolds stress near the wall. *Journal of Fluid Mechanics*, 55:65–92, 1972.

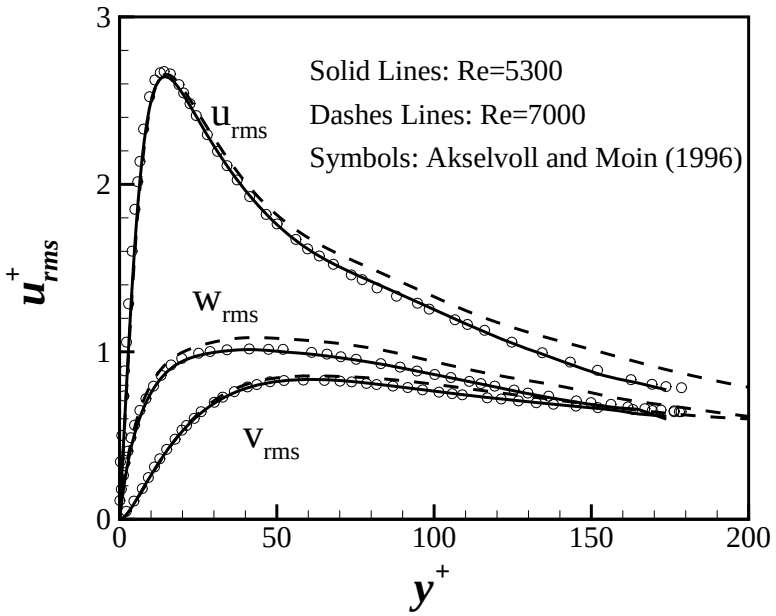

Figure 1: Velocity fluctuations of DNS pipe flow at $Re_D = 5300$. The DNS data of Akselvoll and Moin (1996) are included for comparison.

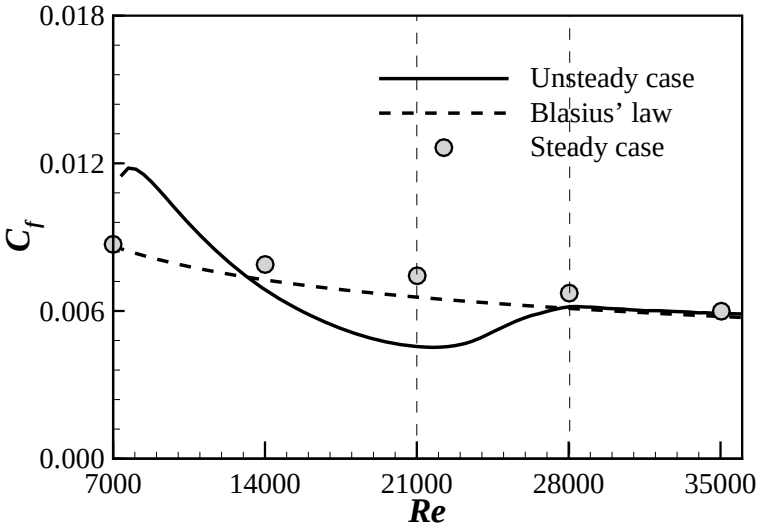

Figure 2: Distribution of skin friction coefficient during the acceleration.

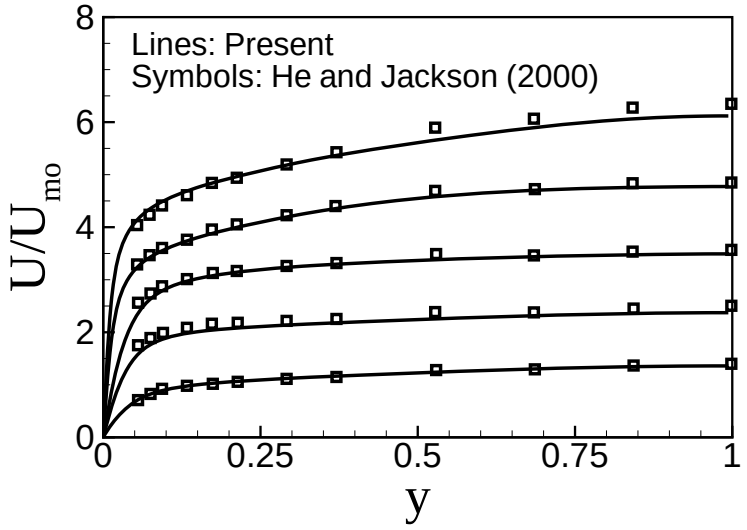

Figure 3: Mean velocity profiles at several Re numbers. Velocity is normalised by the initial bulk-mean velocity, U_{m0}. The Reynolds numbers of the data are $Re_D = 7000$, 14000, 21000, 28000, and 35000.

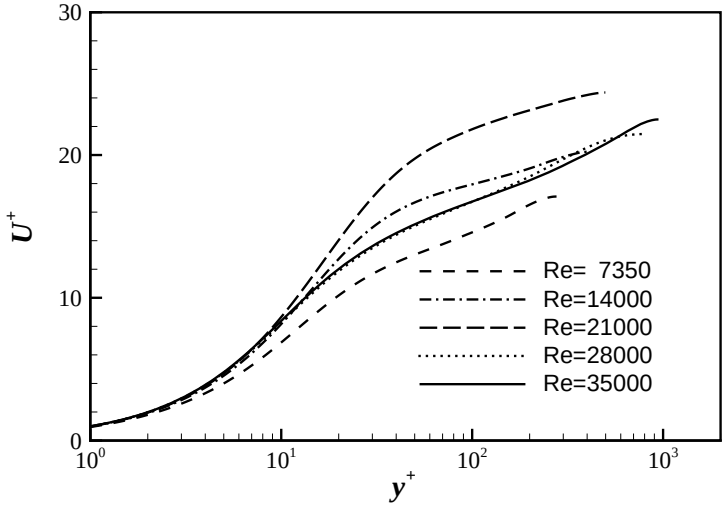

Figure 4: Mean velocity profiles in local wall units, $u^+ = u/u_\tau$ vs. $y^+ = yu_\tau/\nu$, where u_τ is the local friction velocity.

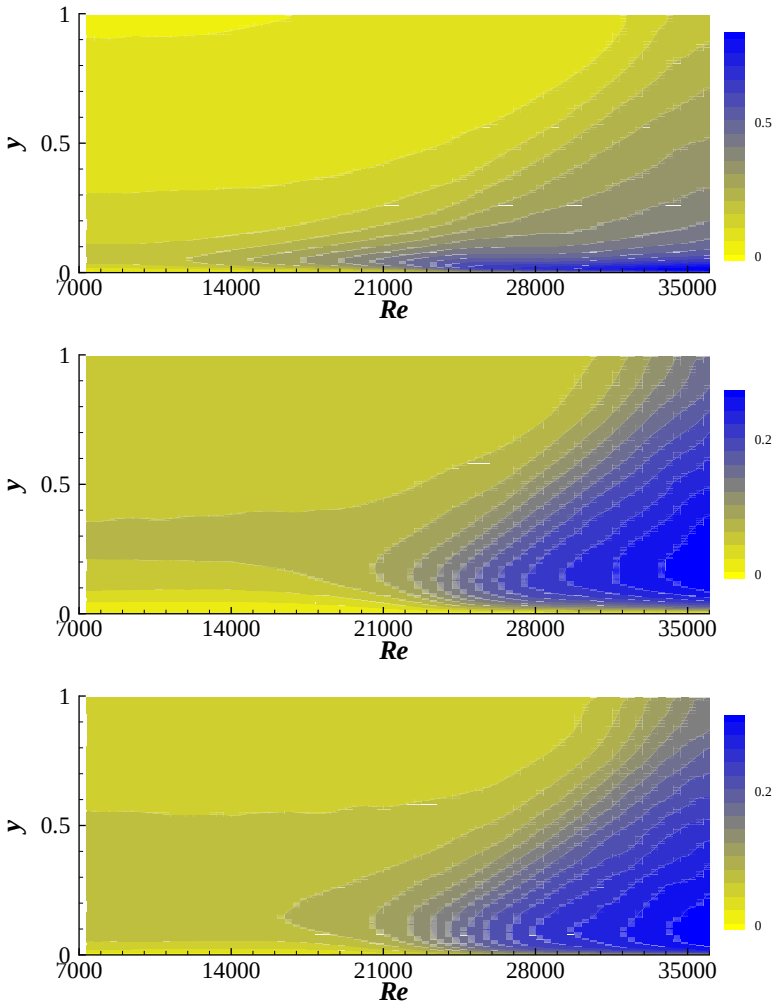

Figure 5: Velocity fluctuations normalised by the initial bulk-mean velocity. a) u_{rms}/U_{m0}, b) v_{rms}/U_{m0}, and c) w_{rms}/U_{m0}.

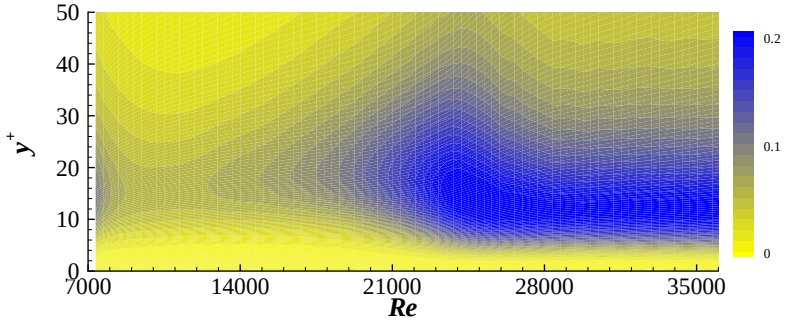

Figure 6: The production term in the turbulence kinetic energy transport equation in local wall units, $-\overline{u'v'}(dU/dy)\nu/u_\tau^4$.

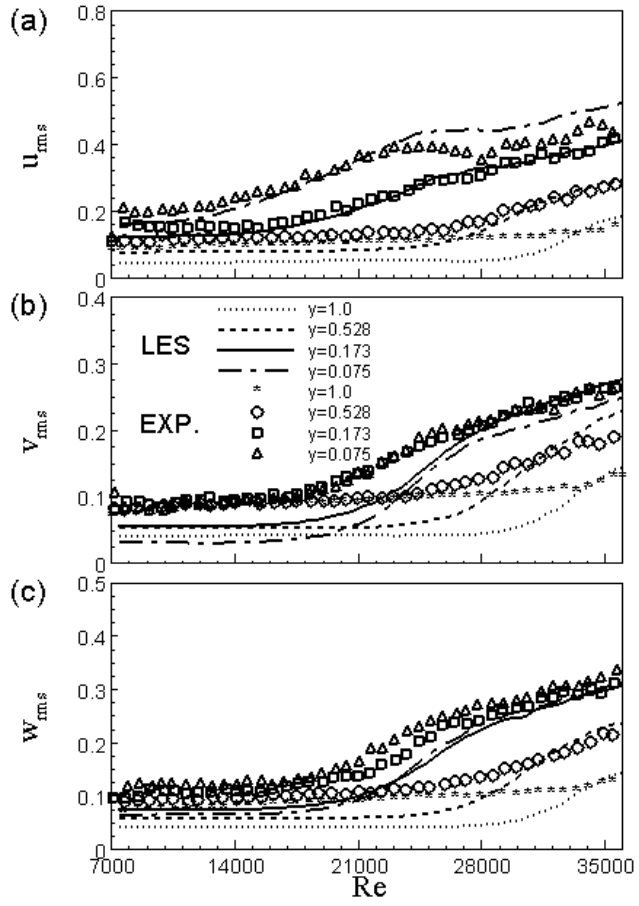

Figure 7: Time history of rms velocity fluctuations. a) u_{rms}, b) v_{rms}, and c) w_{rms}.

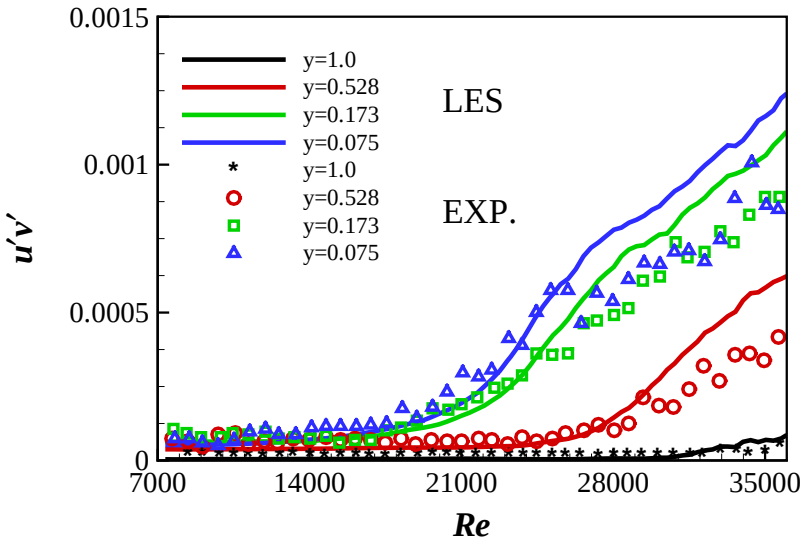

Figure 8: The Reynolds shear stress normalised by the initial bulk-mean velocity, $-\overline{u'v'}/U_{m0}^2$.

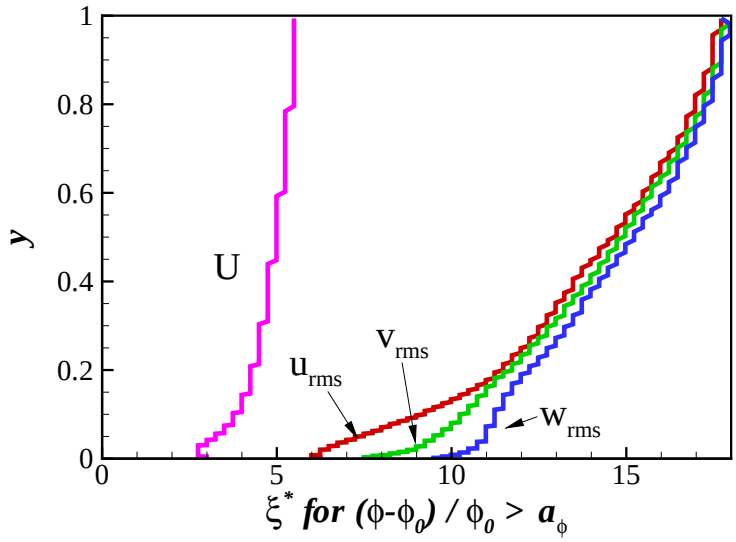

Figure 9: Dimensionless delay time as a function of the distance from the wall.

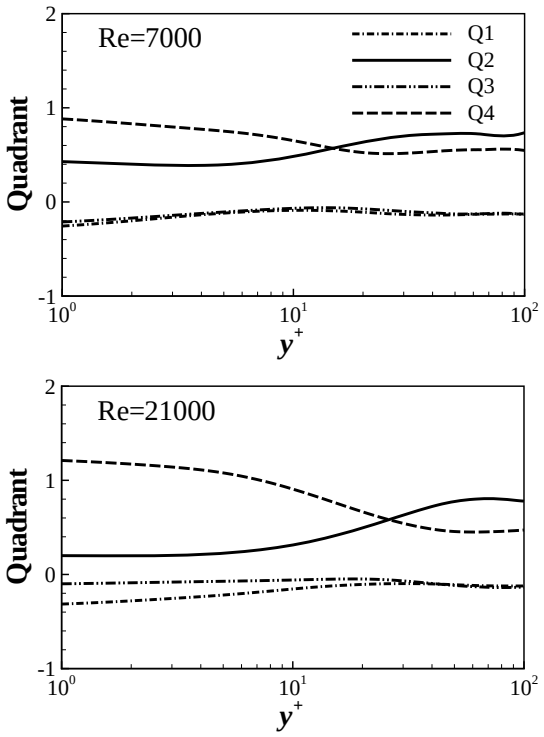

Figure 10: Quadrant analysis for Reynolds shear stress during the acceleration at $Re_D = 7000$ and 21000.

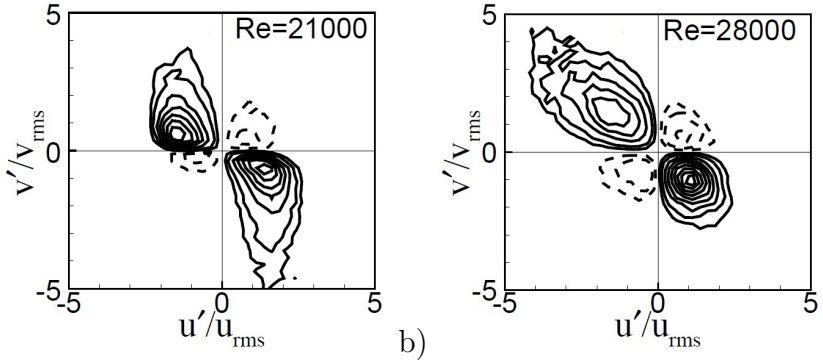

a) b)

Figure 11: Joint weighted probability density functions of velocity fluctuations during acceleration at a) $y = 0.04$, and b) $y = 0.5$.